scientific reports

OPEN

A new family of copper-based MXenes

R. Ponce-Pérez✉, S. J. Gutierrez-Ojeda, J. Guerrero-Sánchez✉ & María G. Moreno-Armenta

In this work, we demonstrate, through first-principles calculations, the existence of a new family of copper-based MXenes. These add up new structures to the previously reported universe and span the interest of such 2D materials for applications in heterogeneous catalysis, ion-based batteries, sensors, biomedical applications, and so on. First, we propose the MXene-like structures: Cu_2N, Cu_2C, and Cu_2O. Phonon spectra calculations confirmed their dynamical stability by showing just positive frequencies all through the 2D Brillouin zone. The new MXenes family displays metallic characteristics, mainly induced by the Cu-3d orbitals. Bader charge analysis and charge density differences depict bonds with ionic character in which Cu is positively charged, and the non-metal atom gets an anionic character. Also, we investigate the functionalization of the proposed structures with Cl, F, O, and OH groups. Results show that the H3 site is the most favorable for functionalization. In all cases, the non-magnetic nature and metallic properties of the pristine MXenes remain. Our results lay the foundations for the experimental realization of a new MXenes family.

Atomic understanding of 2D systems is a critical factor to help in the nanoscale revolution. The hunt for 2D systems with engineered properties has been a constant since the graphene discovery in 2004[1]. To mention, silicene[2], germanene[3], phosphorene[4], borophene[5], and very recently, the plumbene monolayer[6]. All these systems with a great variety of properties and applications. Nevertheless, that is not it. Other binary and ternary 2D materials have emerged as well[7–9], between them, 2D Janus[10] and MXenes[11]. The later with several applications in different fields[12]. It is expected that the MXenes family could be one of the largest in the 2D realm. Since the outbreak work by Michael Naguib et al.[11] on Ti_3C_2, several experimental and theoretical investigations have appeared on different MXenes. For example, antiferromagnetic Cr_2N undergoes a half-metal transition just by adsorbing O on it, being applicable in spintronics[13]. Also, MXenes find applications in next-generation shielding[14], nano-optoelectronics[15], as key to efficient catalytic processes[16], and in energy conversion and storage[17]. So, the spectrum of applications that pristine MXenes bring is still under construction and could be complemented with the addition of new MXene structures. In this way, several research groups are looking for new and novel MXenes with engineered properties through computational and experimental methods[18–26]. MXenes modification through surface functionalization is a possibility. For example, carboxyl functionalized $Ti_3C_2T_x$ MXene shows a high capability to trap and remove U and Eu[20]. Also, sulfur-modified MXenes achieve high storage in Li-ion-based batteries[21].

Mixing two transition metals into the same structure through the formation of either solid solutions or ordered double-transition metal MXenes is another way to engineer the MXenes properties. Ordered double-transition MXene sheets present an optically controlled ferrimagnetic to ferromagnetic transition[23]. Mixed functionalized double MXenes show an antiferromagnetic behavior useful to construct 2D-based spin field-effect transistors[26]. Also, double non-magnetic transition metal MXenes have been used as Li-storage anodes, in which surface storage is enhanced due to the ordered double-transition metal nature of the MXene layer[27].

MXenes are commonly obtained from the precursor MAX phase through selective etching of the A layer, employing aqueous hydrofluoric acid solutions[28]. However, the selective atomic substitution method has been proposed as another way to obtain MXenes. Urbankowski et al.[29] reported the synthesis of Mo_2NT_x and V_2NT_x using as precursors the Mo_2CT_x and V_2CT_x by ammoniation. Sun et al.[30] and Cao et al.[31] synthesized the two-dimensional Mo_5N_6 employing MoS_2 layers as a precursor in a furnace with NH_3 flux, and they demonstrated the versatility of this approach synthesizing W_5N_6. Besides, theoretical investigations have demonstrated that the substitution of M atoms in the MXene phase by other metallic atoms is possible[32,33]; for example, Ti_3C_2 has been modified by substituting Ti atoms with 3d, 4d, and 5d transition metals[32]. The MXenes MCO_2 (M = Ti, V, Zr, Hf, and Ta) were modified by the replacement of the M atom by Cu, Zn, Mo, Ru, Rh, Pd, Ag, Cd, W, Re, Os, Ir, Pt, Au and Hg[33]. Taking into account that MXenes not only come from the MAX phases -they can also be synthesized- opens the door to include more members to the MXenes family.

Centro de Nanociencias y Nanotecnología, Universidad Nacional Autónoma de México, Km. 107, Apdo. 14 Carretera Tijuana-Ensenada, Ensenada, Baja California, Mexico. ✉email: rponce@cnyn.unam.mx; guerrero@cnyn.unam.mx
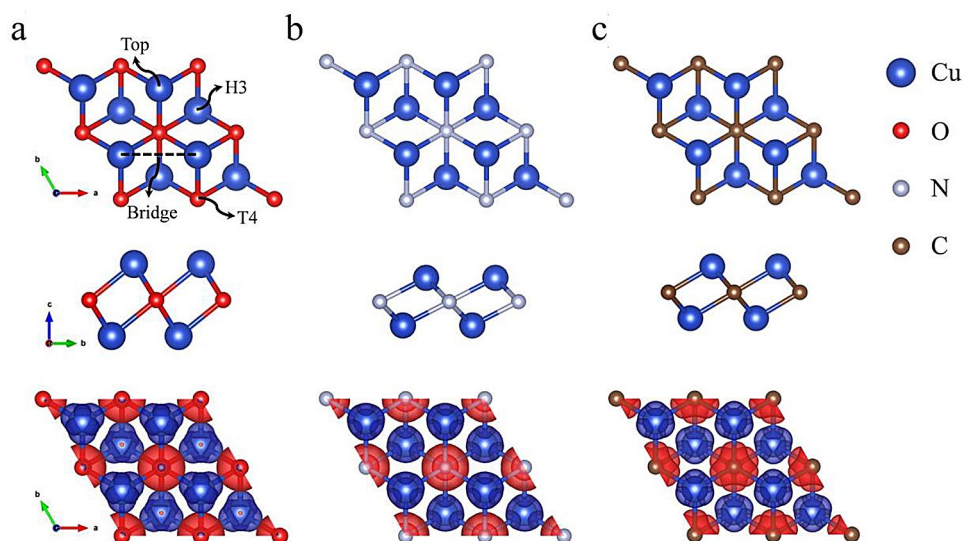
Figure 1. Atomistic representation of the new Cu-based MXene-type structures, the top and side views of (**a**) Cu$_2$O, (**b**) Cu$_2$N, and (**c**) Cu$_2$C. The bottom part represents the electron density difference ($\Delta\rho$). Blue represents depletion, and red is for the accumulation of charge.

Metallic copper has a wide range of applications; due to its high electromigration, it is widely used to construct integrated circuits. Also, Cu is an efficient current collector due to its high electric conduction[34]. Large area and conformal thin Cu films can be achieved on solid surfaces via atomic layer deposition, in which a Cu-based organometallic molecule interacts with the solid surface to generate the growth. The process happens through ligand-exchange reactions[35]. Also, copper surfaces can be used as a substrate to grow graphene, being a natural support to achieve graphene-based electrodes[34].

That is not it; Cu is also widely used in single atom alloy catalysts[36], in which single Pt atoms are incorporated into the Cu surface. Cu generates a high selectivity in hydrogenation processes due to its favored Cu–O interaction with the aldehyde molecules, whereas Pt is the hydrogen source.

We have great expectations of the potential advantages of bringing a 2D material with two exposed Cu surface layers and a large surface area. For example, due to its affinity to graphene, it is natural to think in new vdW heterostructures, which will be highly interesting from the scientific point of view as well as for their potential applications. On the other hand, the feasibility of mixing MXenes with other transition metals assures the formation of single-atom alloy catalysts, in which Pt, Pd, or other relatives can be incorporated. Several other applications related to copper should be expected as well.

Considering the previous discussion, we propose a new copper-based MXenes family: Cu$_2$C, Cu$_2$N, and Cu$_2$O, which are isostructural to the well-known and already studied Cr$_2$C, Cr$_2$N, Ti$_2$C, Ti$_2$N structures[13,32,37,38]. Our results demonstrate that the new MXenes family presents positive frequencies and metallic behavior, even after functionalizing them with Cl, F, O, and OH, a key characteristic that remains from pure copper, pointing out the importance of such 2D structures experimental realization.

Methodology

Calculations on this report were performed using the Vienna Ab initio Simulation Package (VASP)[39–42]. Exchange–correlation energies are treated according to the generalized gradient approximation (GGA) with the Perdew-Burke-Ernzerhof (PBE) parameterization[43]. The electronic states are expanded using the projector-augmented wave basis (PAW)[44,45] with an energy cutoff of 500 eV. The MXene-type structures Cu$_2$X (X = O, N, C) are simulated with the supercell method. A monolayer of Cu$_2$X composes each supercell in a 1 × 1 periodicity and a vacuum space of 15 Å to avoid spurious interactions. In geometry optimization, all force components must be lower than 0.01 eV/ Å and the energy differences less than 1×10^{-4} eV. Integration of electronic states in the Brillouin zone was performed using a Monkhorst–Pack mesh of 15 × 15 × 1 k-points[46]. Phonon dispersions were obtained using the finite-differences method[47] combined with phonopy code[48].

Results

The atomic representation of the new Cu-based MXenes is depicted in Fig. 1. Top and side views of the Cu$_2$O, Cu$_2$N, and Cu$_2$C are shown in Fig. 1a–c, respectively. After full structural optimization without any constraints, the Cu$_2$O, Cu$_2$N, and Cu$_2$C have cell parameters of the order of 2.80, 3.12, and 2.99 Å, respectively. The Cu–O, Cu–N, and Cu–C bonds have distances ~ 2.07, ~ 2.02, and ~ 2.00 Å. Each MXene-type structure comprises two monolayers (ML) of Cu as the most exposed and a central ML of X (X = O, N, C). The Cu-X interlayer distance is 1.30, 0.92, and 1.02 Å for the Cu$_2$O, Cu$_2$N, and Cu$_2$C, respectively.

We calculated the electron density difference ($\Delta\rho$) defined as $\Delta\rho = \rho_{MXene} - \rho_{Cu} - \rho_X$, where ρ_{MXene} is the charge density of the MXene-type structure; ρ_{Cu} and ρ_X are the charge density of the isolated atoms of Cu and X
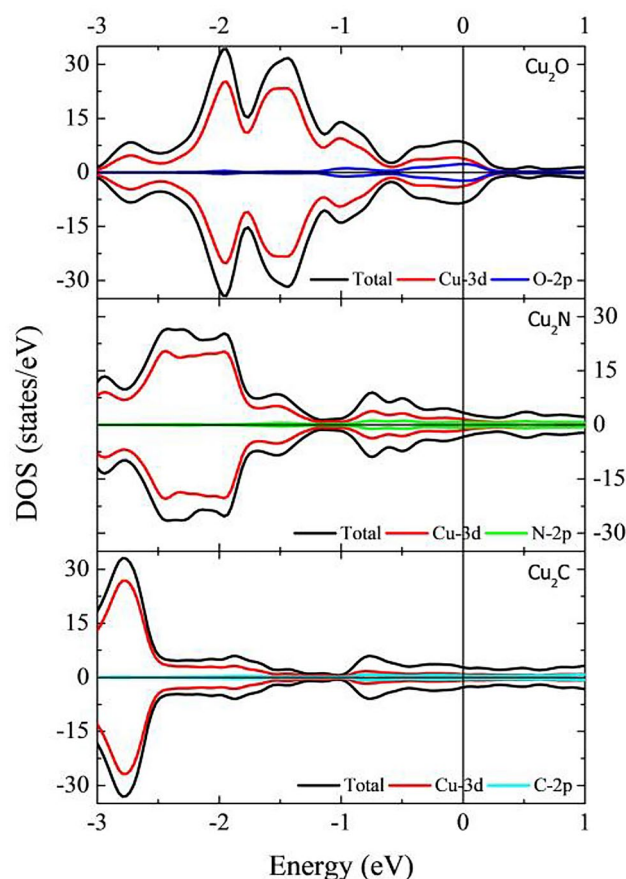
Figure 2. DOS and pDOS for the Cu_2O, Cu_2N and Cu_2C MXenes. Fermi energy is set to 0 eV.

(X = O, N, C) respectively. The isosurfaces for each Cu-based MXene are depicted in Fig. 1, blue color suggests depletion, and the red color corresponds to charge density accumulation. The three different Cu-based MXenes denote charge depletion around the Cu atoms. Also, we observed the accumulation of charge close to the Oxygen atoms. This behavior suggests bonds with ionic behavior. Bader charge density analysis for the Cu_2O MXene-type structure reveals that each Cu atom transfers 0.50e to the three nearest O atoms (0.166e/O); also, each O atom accepts 1.00e from the six Cu nearest neighbors. In the Cu_2N MXene-type structure, Cu atoms donate 0.60e (0.20e/O atom) to the nearest N atoms, which accept 1.20e from the six Cu nearest neighbors. Similar behavior is observed for the Cu_2C MX-type structure, where Cu atoms lose 0.48e (0.16e/O atom) and the O atoms accept 0.96e from the six nearest Cu atoms.

The electronic properties of the new Cu-based MXene-type structures are investigated. The results are summarized in Fig. 2. The density of states (DOS) and projected DOS (pDOS) for the Cu_2O, Cu_2N, and Cu_2C are shown in the upper, middle, and lower panels of Fig. 2, respectively. Fermi level is set as the reference energy in all cases. Positive and negative values along the DOS axis are for spin up and spin down, respectively. In all cases, spin up and spin down show no asymmetry as a clear indication of the material's non-magnetic nature. Also, all the Cu-based MXenes present metallic characteristics. Cu-3d orbitals dominate DOS in all cases, from − 3 to 1 eV, with small contributions coming from the O-2p, N-2p, and C-2p orbitals.

The evidence that demonstrates the possible experimental realization of the Cu-based MXenes is the dynamic stability. In the phonon dispersion, positive frequencies stand for dynamically stable systems, whereas negative values suggest structural instabilities that may need to be corrected using strain or atomic displacements. Here we analyze the phonon dispersions of the new Cu-based MXenes along the path Γ–M–K–Γ (Fig. 3). Dispersions for Cu_2O, Cu_2N, and Cu_2C are shown in Fig. 3a–c, respectively. In all cases, the absence of negative frequencies indicates dynamical stability of the three different Cu-based MXenes.

MXenes are generally obtained with some functional groups attached to them. The most common functional groups are Cl, F, O, and OH. We investigate the surface functionalization of the three different Cu-based MXenes with Cl, F, O, and OH to investigate the change in the electronic properties when functionalizing them.

To evaluate the most favorable site for the functionalization, we considered four high symmetry sites (see Fig. 1a). The Top site corresponds to the site on top of the Cu atom. The T4 site is on top of the central layer atom, H3 is the central point of the hexagon formed by the 1st and second layers, and the Bridge site is the middle point between two Cu atoms of the same layer. According to the calculations, the H3 site is the most favorable configuration in all cases. In general, the H3 site is the most stable functionalization site for all systems, followed
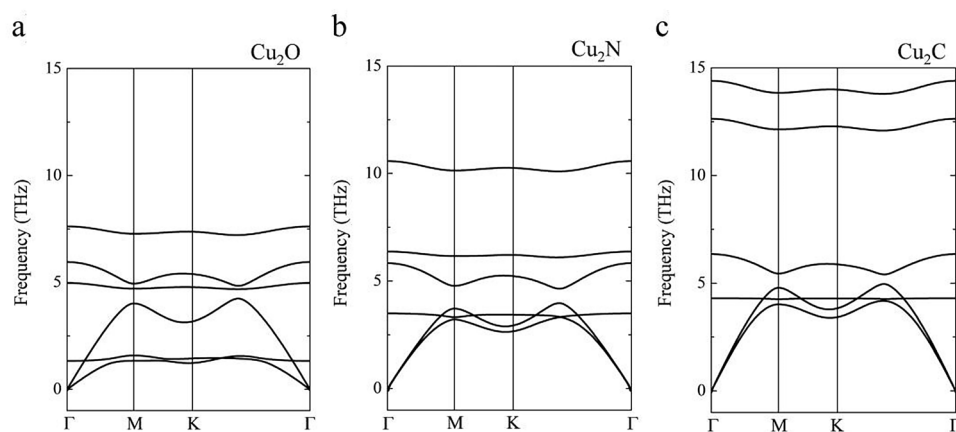
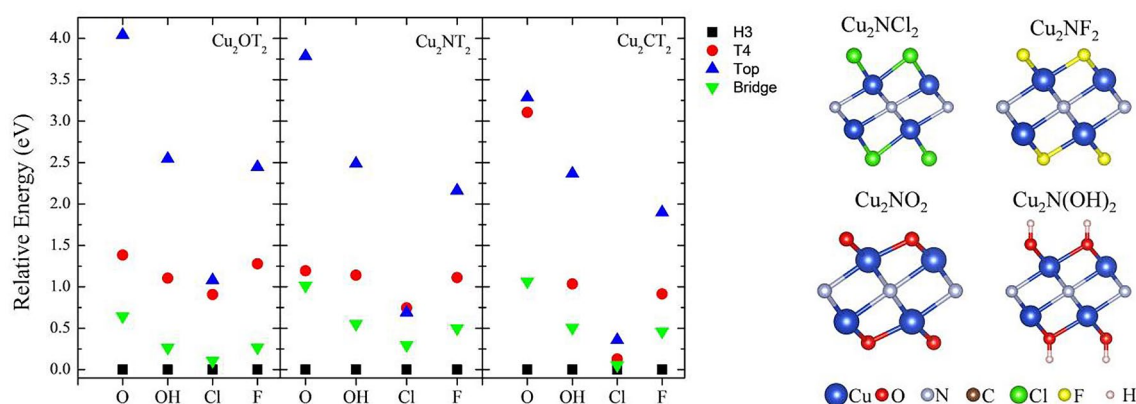**Figure 3.** Phonon dispersion for the Cu-based MXene (**a**) Cu_2O, (**b**) Cu_2N, and (**c**) Cu_2C.

Figure 4. Relative energies for the different Cu_2XT_2 (X = O, C, N and T = Cl, F, O, OH), the atomistic model for the Cu_2NT_2 are shown.

by the bridge site. T4 and Top sites are the least stable (H3 < Bridge < T4 < Top). Relative energies of the different functionalized MXenes are summarized in Fig. 4.

After structural relaxation, the functional groups are threefold coordinated to the Cu atoms. In the case of Cl, the average bond distances with the Cu atoms are 2.36 Å, 2.37 Å, and 2.41 Å, and the interplanar distances are 1.39 Å, 1.45 Å, and 1.48 Å for the Cu_2OCl_2, Cu_2NCl_2, and Cu_2CCl_2, respectively. For functionalization with F atoms, the three different MXenes exhibit the same bond distance (2.04 Å). The interplanar distances are 0.97 Å, 1.07 Å, and 1.10 Å for the Cu_2OF_2, Cu_2NF_2, and Cu_2CF_2, respectively. Similar results are obtained for the Cu_2O_3, Cu_2NO_2, and Cu_2CO_2 MXenes. The Cu–O bond distances are 1.90 Å, 1.91 Å, and 1.94 Å, and the interplanar distances 0.82 Å, 0.83 Å, and 0.78 Å, respectively. Finally, the MXene group functionalized with OH has Cu–O bond distances of the order of 2.07 Å, 2.06 Å, and 2.08 Å. Also, the interplanar distances are 0.99 Å, 1.05 Å, and 1.08 Å for the $Cu_2O(OH)_2$, $Cu_2N(OH)_2$, and $Cu_2C(OH)_2$ MXenes, respectively. The atomistic models for the Cu_2NT_2 (T = Cl, F, O, and OH) are displayed in Fig. 4.

To evaluate the change in electronic properties in the Cu_2XT_2 family due to functionalization, we compute its electronic properties. The DOS and pDOS of the functionalized MXnes are summarized in Fig. 5. In all cases, the energy reference is the Fermi level, positive and negative values along the DOS axis refer to spin up and spin down, respectively. From left to right, the first column depicts the electronic properties of the Cu_2OT_2 (T = Cl, F, O, and OH) functionalized MXenes. Note that in all cases, the non-magnetic nature of the pristine MXene remains. Also, the main contribution to the DOS around the Fermi level comes from the Cu-3d orbitals, followed by contributions of the O-2p orbitals and the T group p-orbitals. Note that the surface functionalization increases the electronic states close to the Fermi level, and therefore the MXenes remain metallic. Similar behavior is obtained for the Cu_2NT_2 (T = Cl, F, O, and OH) functionalized MXenes (central column). Again, functionalized MXenes exhibit metallic characteristics with non-magnetic properties. DOS close to the Fermi is mainly composed of Cu-3d orbitals with a small N-2p and T-p orbitals contribution. The right column depicts the DOS and pDOS of the Cu_2CT_2 (T = Cl, F, O, and OH) functionalized MXenes. Similar to the previous cases, the non-magnetic nature and the metallic behavior of the pristine Cu_2C MXene remain. Around the Fermi level, the main contribution to the DOS comes from the Cu-3d orbitals. C-2p and T-p orbitals contribute to a lesser extent.
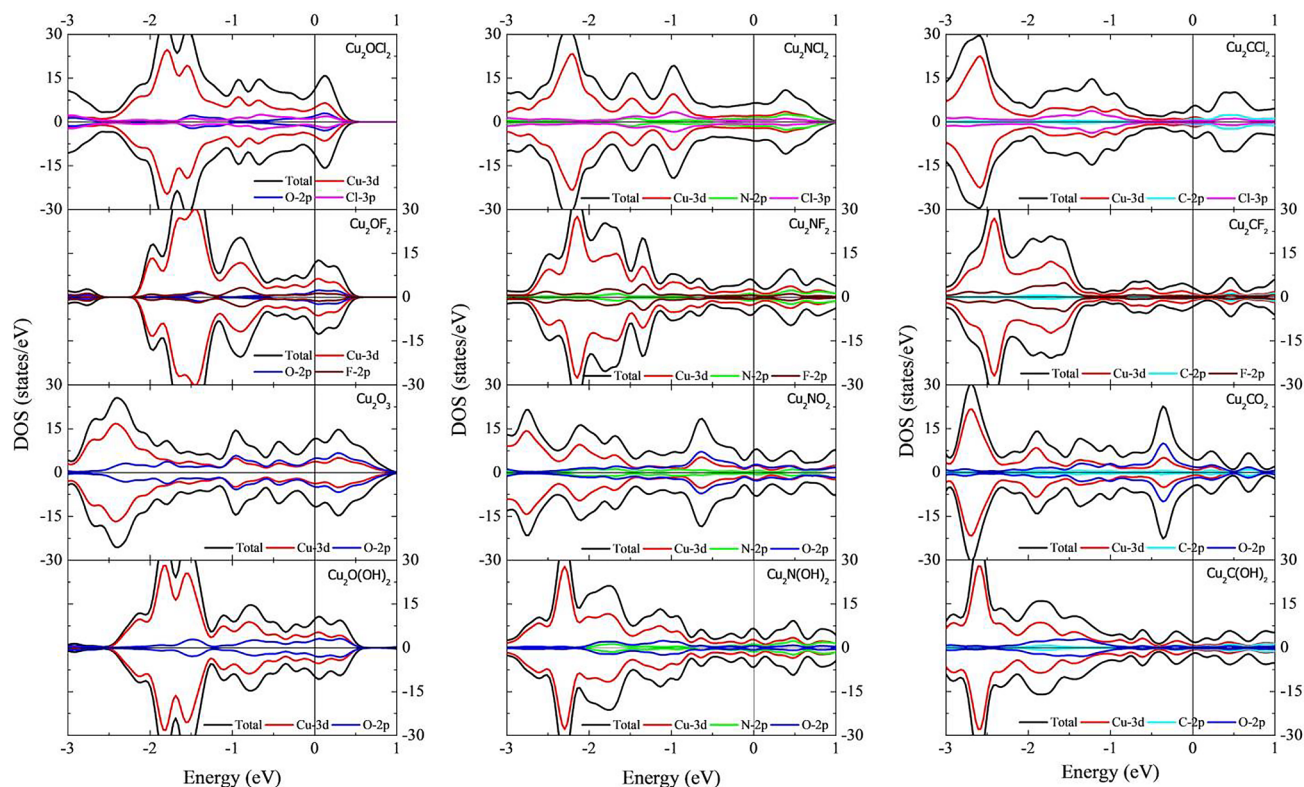
4

Figure 5. DOS and pDOS of the functionalized Cu_2OT_2, Cu_2NT_2 and Cu_2CT_2 (T = Cl, F, O, and OH) MXenes.

Conclusions

In conclusion, by using spin-polarized first-principles total-energy calculations, we predicted the structural and electronic properties of the new Cu-based MXenes Cu_2O, Cu_2N, and Cu_2C. Calculations demonstrate the non-magnetic nature of the MXenes, with metallic characteristics. Functionalization of the proposed MXene structures is carried out employing Cl, F, O and OH groups. Computations show tha all functionalized species are metallic and non-magnetic, similar to the case of pristine MXenes. Also, phonon dispersion with only positive frequencies indicates the dynamical stability of the Cu-based MXenes. Therefore, this new MXenes family could be obtained experimentally, opening an avenue to include the large number of applications that Cu can bring to the realm of 2D materials.

References

1. Novoselov, K. S. *et al.* Electric field effect in atomically thin carbon film. *Science* **306**, 666–669. https://doi.org/10.1126/science.1102896 (2004).
2. Vogt, P. *et al.* Guy le lay, silicene: compelling experimental evidence for graphenelike two-dimensional silicon. *Phys. Rev. Lett.* **108**, 155501. https://doi.org/10.1103/PhysRevLett.108.155501 (2012).
3. Dávila, M. E., Xian, L., Cahangirov, S., Rubio, A. & Le Lay, G. Germanene: a novel two-dimensional germanium allotrope akin to graphene and silicene. *New J. Phys.* **16**, 095002. https://doi.org/10.1088/1367-2630/16/9/095002 (2014).
4. Liu, H. *et al.* Phosphorene: an unexplored 2D semiconductor with a high hole mobility. *ACS Nano* **8**(4), 4033–4041. https://doi.org/10.1021/nn501226z (2014).
5. Mannix, A. J. *et al.* Synthesis of borophenes: anisotropic, two-dimensional boron polymorphs. *Science* **350**, 1513–1516. https://doi.org/10.1126/science.aad1080 (2015).
6. Yuhara, J., He, B., Matsunami, N., Nakatake, M. & Lay, G. L. Graphene's latest cousin: plumbene epitaxial growth on a "nano watercube". *Adv. Mater.* **31**, 1901017. https://doi.org/10.1002/adma.201901017 (2019).
7. Radisavljevic, B., Radenovic, A., Brivio, J., Giacometti, V. & Kis, A. Single-layer MoS2 transistors. *Nat. Nanotechnol.* **6**, 147–150. https://doi.org/10.1038/nnano.2010.279 (2011).
8. Huang, B. *et al.* Layer-dependent ferromagnetism in a van der Waals crystal down to the monolayer limit. *Nature* **546**, 270–273. https://doi.org/10.1038/nature22391 (2017).
9. Gong, C. *et al.* Discovery of intrinsic ferromagnetism in two-dimensional van der Waals crystals. *Nature* **546**, 265–269. https://doi.org/10.1038/nature22060 (2017).
10. Zhang, J. *et al.* *ACS Nano* **11**(8), 8192–8198. https://doi.org/10.1021/acsnano.7b03186 (2017).
11. Naguib, M. *et al.* Two-dimensional nanocrystals produced by exfoliation of Ti3AlC2. *Adv. Mater.* **23**, 4248–4253. https://doi.org/10.1002/adma.201102306 (2011).
12. Gogotsi, Y. & Anasori, B. The rise of MXenes. *ACS Nano* **13**, 8491–8494. https://doi.org/10.1021/acsnano.9b06394 (2019).
13. Wang, G. Theoretical prediction of the intrinsic half-metallicity in surface-oxygen-passivated Cr2N MXene. *J. Phys. Chem. C* **120**, 18850–18857. https://doi.org/10.1021/acs.jpcc.6b05224 (2016).

14. Iqbal, A., Sambyal, P. & Min Koo, C. 2D MXenes for electromagnetic shielding: a review. *Adv. Funct. Mater.* **30**, 2000883. https://doi.org/10.1002/adfm.202000883 (2020).
15. Jiang, X. *et al.* Two-dimensional MXenes: from morphological to optical, electric, and magnetic properties and applications. *Phys. Rep.* **848**, 1–58. https://doi.org/10.1016/j.physrep.2019.12.006 (2020).
16. Morales-García, Á., Calle-Vallejo, F. & Illas, F. MXenes: new horizons in catalysis. *ACS Catal.* **10**(22), 13487–13503. https://doi.org/10.1021/acscatal.0c03106 (2020).
17. Pang, J. *et al.* Applications of 2D MXenes in energy conversion and storage systems. *Chem. Soc. Rev.* **48**, 72–133. https://doi.org/10.1039/C8CS00324F (2019).
18. Zhang, C. *et al.* Two-dimensional transition metal carbides and nitrides (MXenes): synthesis, properties, and electrochemical energy storage applications. *Energy Environ. Mater.* **3**, 29–55. https://doi.org/10.1002/eem2.12058 (2020).
19. Berdiyorov, G. R. & Mahmoud, K. A. Effect of surface termination on ion intercalation selectivity of bilayer Ti3C2T2 (T = F, O and OH) MXene. *Appl. Surf. Sci.* **416**, 725–730. https://doi.org/10.1016/j.apsusc.2017.04.195 (2017).
20. Zhang, P. *et al.* Effective removal of U(VI) and Eu(III) by carboxyl functionalized MXene nanosheets. *J. Hazard. Mater.* **396**, 122731. https://doi.org/10.1016/j.jhazmat.2020.122731 (2020).
21. Wang, X., Cai, Y., Wu, S. & Li, B. Sulfur functions as the activity centers for high-capacity lithium-ion batteries in S- and O-bifunctionalized MXenes: a density functional theory (DFT) study. *Appl. Surf. Sci.* **525**, 146501. https://doi.org/10.1016/j.apsusc.2020.146501 (2020).
22. Zhang, J. J. *et al.* Type-II multiferroic Hf2VC2F2 MXene monolayer with high transition temperature. *J. Am. Chem. Soc.* **140**(30), 9768–9773. https://doi.org/10.1021/jacs.8b06475 (2018).
23. He, J. & Frauenheim, T. Optically driven ultrafast magnetic order transitions in two-dimensional ferrimagnetic MXenes. *J. Phys. Chem. Lett.* **11**(15), 6219–6226. https://doi.org/10.1021/acs.jpclett.0c02007 (2020).
24. He, J., Lyu, P., Sun, L. Z., García, Á. M. & Nachtigall, P. High temperature spin-polarized semiconductivity with zero magnetization in two-dimensional Janus MXenes. *J. Mater. Chem. C* **4**, 6500–6509. https://doi.org/10.1039/C6TC01287F (2016).
25. He, J., Lyu, P. & Nachtigall, P. New two-dimensional Mn-based MXenes with room-temperature ferromagnetism and half-metallicity. *J. Mater. Chem. C* **4**, 11143–11149. https://doi.org/10.1039/C6TC03917K (2016).
26. He, J. *et al.* Cr2TiC2-based double MXenes: novel 2D bipolar antiferromagnetic semiconductor with gate-controllable spin orientation toward antiferromagnetic spintronics. *Nanoscale* **11**, 356–364. https://doi.org/10.1039/C8NR07692H (2019).
27. Syamsai, R. *et al.* Double transition metal MXene (TixTa4−xC3) 2D materials as anodes for Li-ion batteries. *Sci. Rep.* **11**, 688. https://doi.org/10.1038/s41598-020-79991-8 (2021).
28. Salim, O., Mahmoud, K. A., Pant, K. K. & Joshi, R. K. Introduction to MXenes: synthesis and characteristics. *Mater. Today Chem.* **14**, 100191. https://doi.org/10.1016/j.mtchem.2019.08.010 (2019).
29. Urbankowski, P. *et al.* 2D molybdenum and vanadium nitrides synthesized by ammonion of 2D transition metal carbides (MXenes). *Nanoscale* **9**, 17722–17730. https://doi.org/10.1039/C7NR06721F (2017).
30. Sun, G. D., Zhang, G. H. & Chou, K. C. Synthesis of molybdenum nitrides nanosheets by nitriding 2H-MoS2 with ammonia. *J. Am. Ceram. Soc.* **101**, 2796–2808. https://doi.org/10.1111/jace.15467 (2018).
31. Cao, J. *et al.* Realization of 2D crystalline metal nitrides via selective atomic substitution. *Sci. Adv.* **6**, eaax8784. https://doi.org/10.1126/sciadv.aax8784 (2020).
32. Gao, Y. *et al.* Functionalization Ti3C2 MXene by the adsorption or substitution of single metal atom. *Appl. Surf. Sci.* **465**, 911–918. https://doi.org/10.1016/j.apsusc.2018.09.254 (2019).
33. Chen, Z., Huang, S., Huang, B., Wan, M. & Zhou, N. Transition metal atoms implanted into MXenes (M2CO2) for enhanced electrocatalytic hydrogen evolution reaction. *Appl. Surf. Sci.* **509**, 145319. https://doi.org/10.1016/j.apsusc.2020.145319 (2020).
34. Elshazly, M. K., Chang, J. H., Huzayyin, A. & Dawson, F. Influence of Cu(111) and Ni(111) substrates on the capacitances of monolayer and bilayer graphene supercapacitor electrodes. *J. Phys. Chem. C* **123**, 2783–2791. https://doi.org/10.1021/acs.jpcc.8b11211 (2019).
35. Guerrero-Sánchez, J., Takeuchi, N. & Zaera, F. Density functional theory study of the surface adsorption and dissociation of copper(I) acetamidinates on Cu(110) surfaces. *J. Phys. Chem. C* **123**, 4341–4348. https://doi.org/10.1021/acs.jpcc.8b12131 (2019).
36. Cao, Y. *et al.* Controlling selectivity in unsaturated aldehyde hydrogenation using single-site alloy catalysts. *ACS Catal.* **9**, 9150–9157. https://doi.org/10.1021/acscatal.9b02547 (2019).
37. Sun, Q., Fu, Z. & Yang, Z. Tunable magnetic and electronic properties of the Cr-based MXene (Cr2C) with functional groups and doping. *J. Magn. Magn. Mater.* **514**, 167141. https://doi.org/10.1016/j.jmmm.2020.167141 (2020).
38. Soundiraraju, B. & George, B. K. Two-dimensional titanium nitride (Ti2N) MXene: synthesis, characterization, and potential application as surface-enhanced raman scattering substrate. *ACS Nano* **11**, 8892–8900. https://doi.org/10.1021/acsnano.7b03129 (2017).
39. Kresse, G. & Hafner, J. Ab initio molecular dynamics for liquid metals. *Phys. Rev. B* **47**, 558. https://doi.org/10.1103/PhysRevB.47.558 (1993).
40. Kresse, G. & Hafner, J. Ab initio molecular-dynamics simulation of the liquid-metal–amorphous-semiconductor transition in germanium. *Phys. Rev. B* **49**, 14251. https://doi.org/10.1103/PhysRevB.49.14251 (1994).
41. Kresse, G. & Furthmüller, J. Efficiency of ab-initio total energy calculations for metals and semiconductors using a plane-wave basis set. *Comput. Mat. Sci.* **6**, 15–50. https://doi.org/10.1016/0927-0256(96)00008-0 (1996).
42. Kresse, G. & Furthmüller, J. Efficient iterative schemes for ab initio total-energy calculations using a plane-wave basis set. *Phys. Rev. B* **54**, 11169. https://doi.org/10.1103/PhysRevB.54.11169 (1996).
43. Perdew, J. P., Burke, K. & Ernzerhof, M. Generalized gradient approximation made simple. *Phys. Rev. Lett.* **77**, 3865. https://doi.org/10.1103/PhysRevLett.77.3865 (1996).
44. Blochl, P. E. Projector augmented-wave method. *Phys. Rev. B* **50**, 17953. https://doi.org/10.1103/PhysRevB.50.17953 (1994).
45. Kresse, G. & Joubert, D. From ultrasoft pseudopotentials to the projector augmented-wave method. *Phys. Rev. B* **59**, 1758. https://doi.org/10.1103/PhysRevB.59.1758 (1999).
46. Monkhorst, H. & Pack, J. Special points for Brillouin-zone integrations. *Phys. Rev. B* **13**, 5188–5192. https://doi.org/10.1103/PhysRevB.13.5188 (1976).
47. Chaput, L., Togo, A., Tanaka, I. & Hug, G. Phonon-phonon interactions in transition metals. *Phys. Rev. B* **84**, 094302. https://doi.org/10.1103/PhysRevB.84.094302 (2011).
48. Togo, A. & Tanaka, I. First principles phonon calculations in materials science. *Scr. Mater.* **108**, 1–5. https://doi.org/10.1016/j.scriptamat.2015.07.021 (2015).

Acknowledgements

Author contributions

Credit author statement R.P-P.: investigation, methodology, formal analysis, Writing—Original Draft; S.J.G-O.: Writing—Review & Editing; J.G-S.: formal analysis, Writing—Original Draft software, resources; M.G.M-A.: software, resources, Writing—Review & Editing supervision.

Competing interests

The authors declare no competing interests.

Additional information

Correspondence and requests for materials should be addressed to R.P.-P. or J.G.-S.

Reprints and permissions information is available at www.nature.com/reprints.

Publisher's note Springer Nature remains neutral with regard to jurisdictional claims in published maps and institutional affiliations.